Microstructural Aspects of Second Phases in As-cast and Homogenized 7055 Aluminum Alloy with Different Impurity Contents

HUAN SHE, DA SHU, WEI CHU, JUN WANG, and BAODE SUN

The microstructural factors such as type, area fraction, morphology, distribution, and size of second phases in as-cast and homogenized 7055 aluminum alloy and the influence of impurity content variations have been investigated by using optical microscope (OM), scanning electron microscope (SEM), energy dispersive X-ray analysis (EDS), and X-ray diffraction (XRD). In as-cast microstructures, the dominant second phases of η [Mg(Al, Cu, Zn)$_2$] with extended solubility of Cu and Al, a small amount of impurity phases of Al_7Cu_2Fe and Al_3Fe with a little solubility of Cu and Si, and trace Mg_2Si are identified. The variations of Fe and Si contents have no significant influence on the area fraction of η phases, but the area fraction of Fe-rich phase decreases from 0.231 to 0.102 pct with Fe content decreasing from 0.080 to 0.038 wt pct. Decreasing Fe contents reduces the size parameters of Fe-rich phases and refines their morphology correspondingly. After being homogenized at 753 K (480 °C) for 24 hours, η phases are largely dissolved, but the coarse impurity phases are insoluble. Compared with as-cast microstructures, the area fraction and composition of Fe-rich phases change a little but their morphologies are slightly coarsened.

DOI: 10.1007/s11661-013-1709-8

I. INTRODUCTION

7XXX series aluminum alloys (Al-Zn-Mg-Cu) are widely used in aerospace industry because of their high specific strength.[1] To meet the demand of a superior combination of high strength, fracture toughness, and stress corrosion cracking resistance for aircraft materials, one of the important approaches has been to reduce the contents of impurity elements such as Fe and Si in alloy compositions.

During casting of Al-Zn-Mg-Cu alloys, Fe and Si impurities give rise to the formation of coarse intermetallic particles such as Al_7Cu_2Fe, Al_3Fe, α-AlFeSi, and Mg_2Si with sizes larger than 1 μm at the grain boundaries.[2] Because of higher melting points, those coarse particles are insoluble during subsequent heat and thermomechanical treatments.[3,4] Moreover, thermomechanical treatments such as rolling or extrusion with a limited amount of deformation are difficult to fragment them to very small.[5] Therefore, they remain in commercial plates, sheets, and extrusions to deteriorate the toughness and stress corrosion cracking (SCC) resistance of materials. The coarse intermetallic particles, especially the Fe-rich and Si-rich phases are brittle, hard, and incoherent with the α-Al matrix. Thus, they are easy to crack or separate from the matrix to form voids at a low stress, which then grow and link under the loaded stress, finally form the macrocrack to cause the fracture of the alloys.[6,7]

The effects of Fe and Si impurities on the SCC resistance are relative to the pitting of Fe-rich and Si-rich phases in Al-Zn-Mg-Cu alloys,[8,9] which are found to be the initial site for localized corrosion due to the difference of Volta potential causing the strong galvanic coupling forming with the surrounding matrix.[10] Besides, the coarse phases containing Cu and Fe are cathodes with respect to the matrix and promote dissolution of the matrix, while the phases rich in Mg are anodes with respect to the matrix and dissolve preferentially.[9] Anodic dissolution not only provides an initial crack[11] but also promotes the production of hydrogen on the cathode,[12] hence reducing the SCC resistance.

The fracture toughness may be decreased due to the increase of volume fraction of coarse Fe-rich and Si-rich phases with increasing Fe and Si contents, while the strength and elongation are virtually independent of Fe and Si contents in Al-Zn-Mg-Cu alloys.[13–16] Even though the harmful impact of Fe and Si impurities on the microstructures and properties of Al-Zn-Mg-Cu alloys has been reported, less attention has been focused on the evolution of second phases in as-cast and homogenized alloys with variations of Fe and Si contents, especially for ultra-high strength aluminum alloys.

The aim of this work is to characterize the microstructural factors of the second phases, especially Fe-rich phases, present in as-cast and subsequently homogenized microstructures of ultrahigh-strength 7055 aluminum alloy with different levels of Fe and Si contents within its specification range.

HUAN SHE, Doctoral Student, DA SHU, Associate Professor, WEI CHU, Master Student, and JUN WANG and BAODE SUN, Professors, are with the State Key Laboratory of Metal Matrix Composites, Shanghai Jiao Tong University, Shanghai 200240, P.R. China. Contact e-mail: dshu@sjtu.edu.cn
Manuscript submitted November 20, 2012.
Article published online April 12, 2013

II. EXPERIMENTAL PROCEDURE

Commercial-purity aluminum (99.7 wt pct) and high-purity aluminum of 99.99 wt pct (4N) and 99.999 wt pct (5N) were used as raw materials to prepare three 7055 aluminum alloys with a nominal composition of Al-8.4 wt pct Zn-2.3 wt pct Mg-2.4 wt pct Cu-0.15 wt pct Zr but with different impurity contents (designated alloys 1, 2, and 3), respectively. Other alloying elements were respectively added by pure zinc (99.995 wt pct), pure magnesium (99.8 wt pct), Al-5 wt pct Zr, and Al-50 wt pct Cu master alloys. All the raw materials were degreased, acid pickled, and alkaline cleaned to remove the surface dirt and oxide layer, then dried before alloying. For each composition, a 4-kg charge of raw materials was melted in an induction melting furnace with a graphite crucible, held for 2 hours, and then cast into an ingot of $\phi 146 \times 80$ mm in another graphite crucible. Before heating, the furnace was prevacuumized and then filled with argon. The processes of melting and casting were under protection with argon. The ingots were homogenized at 753 K (480 °C) for 24 hours and then quenched in water at room temperature.

The chemical compositions of the alloys prepared were determined by inductively coupled plasma (ICP) spectrometry. Small specimens (approximately 1 cm × 1 cm × 1 cm for each) were cut from each ingot in the center and edge of the section with 2/3 height from the bottom, respectively, used to observe and analyze the as-cast and homogenized microstructures. After mechanical grounding and polishing, some specimens were etched with NaOH aqueous solution for observing dendritic structure using an optical microscope (OM), while unetched specimens were used for analyzing the type, morphology, and distribution of the second phases present in 7055 alloys by OM, scanning electron microscopy (SEM) and energy-dispersive X-ray spectrometry (EDS). The area fraction and size of coarse intermetallic particles were quantitatively measured over a number of optical micrographs using an image analysis software. Besides, X-ray diffraction (XRD) analysis was undertaken to identify the alloy phases present in as-cast alloys.

III. RESULTS AND DISCUSSION

A. *Source Analysis of Impurities in 7055 Aluminum Alloys*

The chemical compositions of the alloys prepared with commercial-purity aluminum and 4N and 5N high-purity aluminum are given in Table I. All the elemental compositions fall into the specification range of 7055 alloy, with a total impurity content of 2220, 1332, and 1208 ppm for alloys 1, 2, and 3, respectively. Fe and Si elements are the dominant impurities in the three 7055 alloys, while the other impurity contents are very low.

The impurity contents brought into 7055 alloys by different raw materials were calculated, respectively, summed, and compared with the measured values as shown in Figure 1. The impurity contents of Al-5 wt pct Zr and Al-50 wt pct Cu master alloys were also determined by inductively coupled plasma (ICP) spectrometry. For alloy 1, nearly 90 pct of the impurity contents was from the raw material of commercial purity aluminum. On the contrary, for alloy 2 and alloy 3, the calculated impurity contents from the raw materials of high-purity aluminum were very small, while the dominant impurity contents came from the raw materials of Al-5 wt pct Zr and Al-50 wt pct Cu master alloys. In alloys 2 and 3, the calculated total impurity contents are significantly less than experimental results, indicating the occurrence of contamination from crucibles or tools during the melting and casting process. It demonstrates that if aims are to prepare higher purity 7055 aluminum alloy, not only the impurity contents in the raw material of pure Al but also in the raw materials of master alloys and contamination from crucibles or tools should be strictly controlled.

B. *Second-Phase Analysis*

1. *Second Phases Present in 7055 Aluminum Alloys*

Optical microscopy reveals that the three as-cast 7055 alloys have similar dendritic microstructure of primary α(Al)-solid solution surrounded by interdendritic second phases, as shown in Figure 2. The difference between the center and edge microstructures results from the distinct cooling rate at the center and edge in the ingot.[17]

Figure 3(a) shows that the as-cast microstructures consist of several coarse second phases with different grayscales in alloy 1. The second phases of alloys 2 and 3 have similar grayscale, distribution, and composition with that of alloy 1. The light-gray phase is the dominant second phase, most of which distributes at grain boundaries and form continuous network, but a few of which distribute within grains as granular or discontinuous strip. The gray phase with a smaller amount exists mostly at the grain boundaries as needle and strip, with a few within grains, and usually it occurs together with the light-gray phase. Another second phase with the least amount is the black phase, present generally at the grain boundaries as a strip, and it can be only observed in alloy 1. The distribution of the gray and black phases is not uniform. Some regions are free

Table I. Chemical Compositions of Prepared 7055 Aluminum Alloys with Different Impurity Contents (Weight Percent)

Alloy No.	Fe	Si	Zn	Mg	Cu	Mn	Cr	Ti	Zr	Al
1	0.080	0.054	8.261	2.136	2.062	0.002	0.001	0.004	0.155	Bal.
2	0.038	0.006	7.794	2.057	2.045	0.001	0.003	0.003	0.146	Bal.
3	0.030	0.008	8.235	2.188	2.119	0.002	0.002	0.003	0.158	Bal.

of these phases but others are observed with an aggregation.

Figures 3(b) through (d) show the SEM images of the typical second phases present in alloy 1, the compositions of which were determined by EDS analysis as shown in Table II. Almost all the coarse light-gray phases have the similar composition with a concentration of 25.03 at. pct Al, 22.18 at. pct Zn, 36.96 at. pct Mg, and 15.83 at. pct Cu. In Al-Zn-Mg-Cu alloys, the main alloying elements Zn, Mg, and Cu can form $\eta(MgZn_2)$, $T(Al_2Mg_3Zn_3)$, $S(Al_2CuMg)$, and $\theta(Al_2Cu)$ phases depending on the alloy chemistry, and η, T, and S can precipitate as three eutectic structures with α-Al *viz.* α-Al/η, α-Al/T, and α-Al/S.[2,5,18–21] Cu and Al atoms can be dissolved in η phase substituting for Zn atoms at the Zn sublattice to form a quaternary phase of (Cu, Zn, Al)$_2$Mg, which is isomorphous with $MgZn_2$.[19,21] Besides, T phases have extended solubility of Cu in them, while S phase shows metastable solubility of Zn.[18,19,22] When the addition of Cu is below 2.5 wt pct, most of Cu are dissolved in η and T phases. However, above 2.5 wt pct, Cu tends to form S phase rather than dissolving in the matrix or in η and T phases. The θ phase can be observed in the alloys with high Cu/Mg ratio; moreover, Mg and Zn atoms are insoluble in θ phase.[18,23]

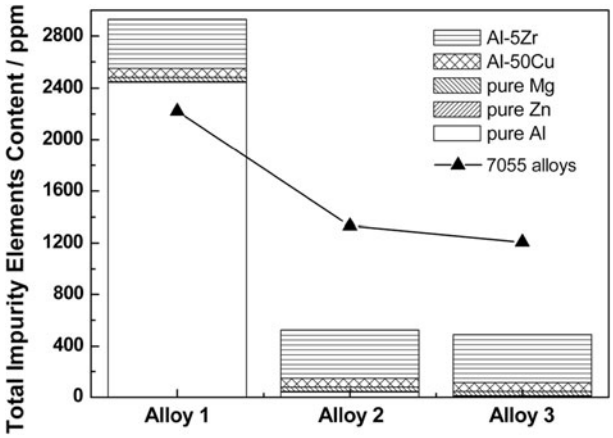

Fig. 1—Source analysis of the impurities in prepared 7055 alloys brought by raw materials.

For the light-gray phase here, it should not be S phase because the atomic fraction of Zn is higher than that of Cu in this phase, while the atomic fraction of Zn is much lower than that of Cu and Mg in S phase reported in literatures.[4,20,24,25] In addition, the atomic fraction of Mg is higher than that of Al in the light-gray phase, which is contrary to the stoichiometric composition of S (Al_2CuMg) phase. Therefore, it might be T phase with extended solubility of Cu or η phase with dissolution of Cu and Al. However, T phase and η phase cannot be distinguished under an optical microscope because of their similar grayscale[19] and cannot be completely identified by EDS analysis. Figure 4 shows XRD analysis results to further identify the second phases. From the XRD patterns, it can be confirmed that the three as-cast 7055 alloys have the same type of phases and the dominant second phase (*viz.* the coarse light gray phase) is η phase besides α-Al, with a few T phase. Figure 3(b) also shows that most of the coarse η phase is present in the form of lamellar eutectic structure with α-Al, but separate η phase skeletons are also found beside the α-Al/η eutectic.

From the EDS results, the gray phase is rich in Al, Cu, and Fe elements with a Cu/Fe ratio of nearly 1:1. It is well known that the solubility of Fe in aluminum alloy is very small and it usually presents as Al_3Fe.[26] But in the alloys with high Cu content, the stable Fe-rich phase

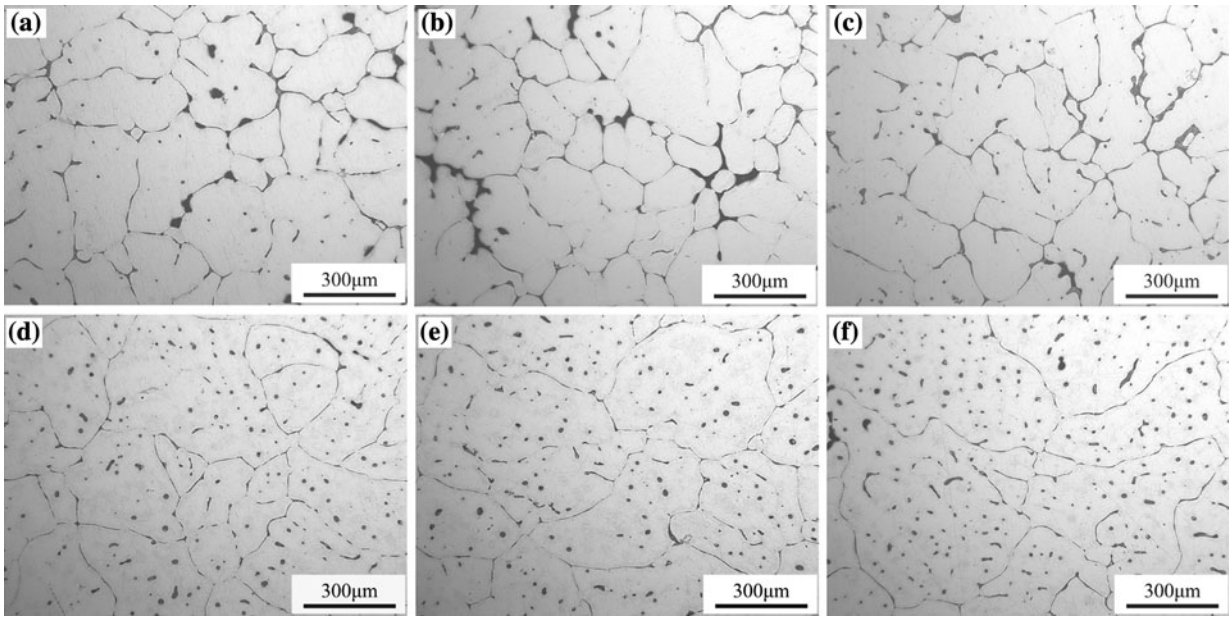

Fig. 2—Optical microstructures of as-cast 7055 alloys with etched (*a*) through (*c*) center, (*d*) through (*f*) edge, (a and d) alloy 1, (b and e) alloy 2, (c and f) alloy 3.

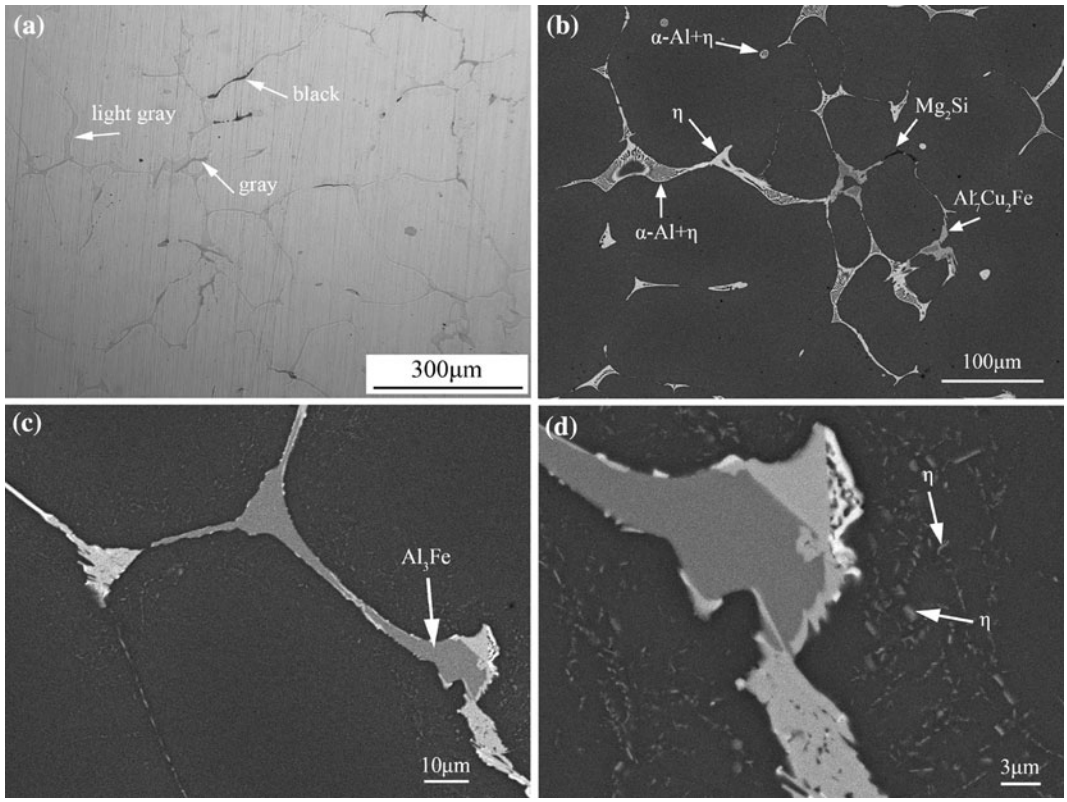

Fig. 3—The center microstructures of alloy 1 (polished without etched) (*a*) optical microstructures, backscattered electron (BSE) images showing (*b*) morphology of different second phases present in as-cast microstructures, (*c*) dark-gray Al_3Fe phase, and (*d*) dispersed η phase magnified in (c).

Table II. Chemical Compositions of Second Phases Present in As-Cast 7055 Alloys (at. pct)

Second Phases	Mg	Zn	Cu	Fe	Si	Al
Coarse η	36.96	22.18	15.83	n/a	n/a	25.03
Al_7Cu_2Fe	n/a	n/a	14.1	17.68	n/a	68.22
Al_3Fe	n/a	n/a	2.75	22.97	1.37	72.92
Mg_2Si	60.72	n/a	n/a	n/a	39.28	n/a
Dispersed η	3.15	6.92	n/a	n/a	n/a	89.94

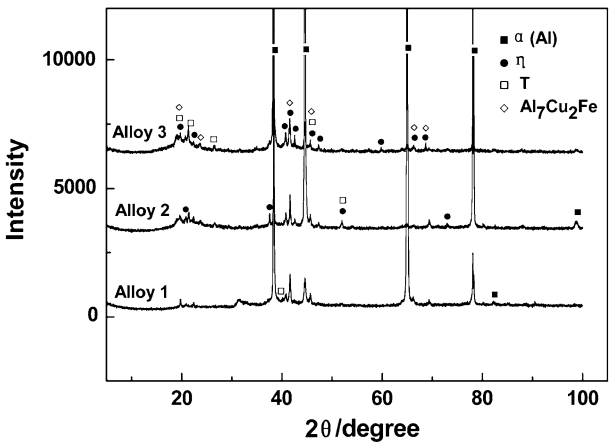

Fig. 4—XRD patterns of the as-cast alloys.

is transformed to Al_7Cu_2Fe.[22] In many 7*xxx* alloys with Cu, *e.g.*, 7075, 7050, and 7A55, Al_7Cu_2Fe has been found as the main impurity phase.[4,22,24,27,28] Therefore, the gray phase can be inferred as Al_7Cu_2Fe, although the Cu/Fe ratio measured is lower than its stoichiometric one, which is similar to the research of Li *et al.*[22] The presence of Al_7Cu_2Fe phase is also confirmed by the XRD analysis shown in Figure 4.

In a similar way, the black phase can be identified as Mg_2Si. In addition, there are two other types of second phases found by SEM, as shown in Figures 3(c) and (d), which were not observed in the optical micrographs. Within the dark-gray phase shown in Figure 3(c), an EDS analysis shows that a small amount of Si was present and the atomic fraction of Fe increases, but the atomic fraction of Cu decreases obviously compared with Al_7Cu_2Fe, as shown in Table II. It can be asserted as Al_3Fe phase with solution of Cu and Si. It has been reported that in Al_3Fe phase, the solubility limit of Cu is about 6 at. pct by replacement of Al atoms and Si also has a small solubility.[29,30] The absence of Mg_2Si phase in alloys 2 and 3 is due to the reduction of Si content by nearly one order of magnitude compared to alloy 1. The

trace Si element beyond its solid-solution limit in α-Al in alloys 2 and 3 is preferentially dissolved in the Al_3Fe phase other than in combination with Mg to form Mg_2Si phase.[21] It may be inferred that the coarse Mg_2Si phase cannot be formed during solidification in 7055 alloys when the Si content is lower than 80 ppm.

Figure 3(d) shows that the gray Al_7Cu_2Fe phase is around the dark-gray Al_3Fe phase, and meanwhile, it is surrounded by the light-gray η phase, denoting that Al_7Cu_2Fe may heterogeneously nucleate on Al_3Fe phase and in turn help nucleate η phase. The sequence of the three phases formed during solidification is accordant with the modeling result of Xie *et al.*'s study[21] for 7050 alloy that Al_7Cu_2Fe is formed after Al_3Fe but before the dominant second phase composed by the main alloying elements Zn, Mg, and Cu. It was reported that trace levels of Fe have a distinct effect on the nucleation of eutectic structure, but the role of Fe-rich phase remains unresolved.[31]

In Figure 3(d), bands of fine dispersoid particles are visible around the η phase. An EDS analysis shows these particles are rich in Zn and Mg (as shown in Table II) with a Mg/Zn ratio of about 2:1; thus, they can be determined as η phase. They might precipitate from α-Al matrix during cooling due to the decrease of solubility with decreasing temperature rather than from liquid. The morphology and distribution of η precipitates in this study agree with the study of Robson.[4]

After being homogenized at 753 K (480 °C) for 24 hours, all the dispersed η precipitates were completely dissolved into the matrix and the majority of the coarse η phase was dissolved, whereas the Fe-rich phases still remained in the homogenized microstructures, as shown in Figure 5. Moreover, the compositions of Fe-rich phases in homogenized microstructures detected by EDS analysis given in Table III are similar to those in as-cast microstructures. In Al-Zn-Mg-Cu alloys, Fe-rich phases have higher melting points than the eutectics, and the solubility limits of Fe and Si in α-Al are scarce, causing difficulty in dissolving during homogenization.[4,5] It has been reported by Eivani *et al.*[3] that $Al_{13}Fe_4$ and Al_8Fe_2Si in AA7020 begin to dissolute when the homogenized temperature reaches 783 K (510 °C).

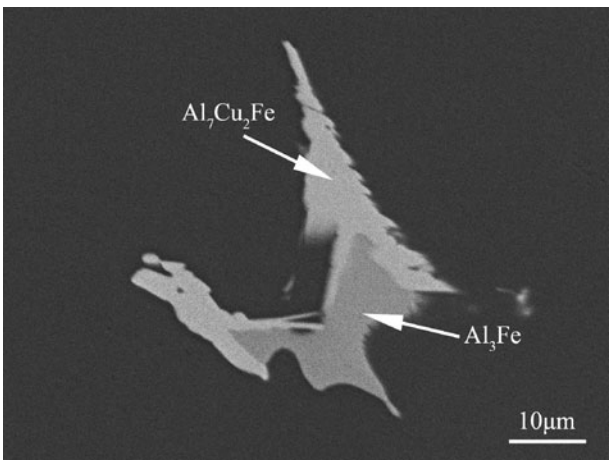

Fig. 5—The residual Fe-rich phase in homogenized microstructures of alloy 1 (polished without etched, BSE image).

2. *Quantitative Analysis of Coarse Intermetallic Phases*

The insoluble Fe-rich phases, such as Al_7Cu_2Fe and Al_3Fe, are known to be particularly detrimental to material properties, *e.g.*, the fracture toughness and fatigue property depends to a large extent on the volume fraction and size of these insoluble particles.[6,13,16] The microstructural parameters of coarse η phase and Fe-rich phases in as-cast and homogenized 7055 aluminum alloys with different impurity contents were quantitatively measured and counted by using an image analysis software, including the area fraction f_A of η phase and Fe-rich phases, and the size of Fe-rich phases expressed by the average length L, the maximum length L_{max}, the minimum length L_{min}, the average width W, the maximum width W_{max}, the minimum width W_{min}, and the average length–width ratio λ, as shown in Table IV.

In as-cast 7055 alloys, the area fraction of η phase is relatively unaffected by the variations of Fe and Si contents, while the area fraction and size of Fe-rich phases are dependent on the Fe content. The area fraction of Fe-rich phases is decreased by 55.8 pct, from 0.231 pct to 0.102 pct, with decreasing Fe content from 0.080 wt pct to 0.038 wt pct. When the Fe content is further decreased to 0.030 wt pct in alloy 3, the area fraction of Fe-rich phases is not decreased correspondently. The size parameters of L, L_{max}, L_{min}, W, W_{max}, W_{min}, and λ of Fe-rich phases are also reduced with decreasing Fe content in as-cast alloys. It is illustrated that the size of Fe-rich phases are refined and their morphology is modified from long needle or strip to short needle, strip or granular particles with decreasing Fe content.

The evolution of microstructural parameters (*e.g.*, content, size, and morphology) of Fe-rich phases is attributed to the influence of Fe content on the nucleation and growth of Fe-rich phases. As shown in Figure 3, almost all the Fe-rich phases are distributed at interdendrites or grain boundaries, which are the finally solidified positions of the ingots. It is well known that the solid solubility of Fe in α-Al is very small and the diffusion coefficient is low both in solid and liquid Al,[5,26,32] which results in the segregation of Fe element at interdendrites and grain boundaries under the non-equilibrium solidification. With lower Fe content, the less segregation extent of Fe makes the nucleation of Fe-rich phases more difficult and its growth much slower, leading to the refinement of the Fe-rich phases. The reduction of alloy element contents segregated at grain boundaries, which decreases the content of second phases distributed at grain boundaries and makes them smaller is also observed in Zuo *et al.*'s report.[17]

The area fraction of Fe-rich phases in homogenized microstructure exhibits a minor difference from that in the as-cast microstructure for alloy 1 and alloy 2, but it decreases a little for alloy 3. Nevertheless, after homogenization, L and L_{max} decrease for alloy 1 but increase for alloy 2 and alloy 3, while W and W_{max} increase and λ decreases for all alloys. The variations in microstructural

Table III. Chemical Compositions of Fe-rich Phases Present in Homogenized 7055 Alloys (at. pct)

Fe-Rich Phases	Cu	Fe	Si	Al
Al_7Cu_2Fe	14.55	18.91	n/a	62.26
Al_3Fe	4.65	25.60	3.10	66.65

Table IV. Microstructural Parameters of Coarse η Phase and Fe-rich Phases in As-cast and Homogenized 7055 Aluminum Alloys with Different Impurity Contents

Alloys	η Phase	Fe-Rich Phases							
	f_A (pct)	f_A (pct)	L (μm)	L_{max} (μm)	L_{min} (μm)	W (μm)	W_{max} (μm)	W_{min} (μm)	λ
As-cast									
1	2.31	0.231	30.5	161.8	2.02	3.67	28.8	0.1	14.2
2	2.28	0.102	19.4	95.8	2.71	3.62	13.4	0.1	9.1
3	2.72	0.104	17.3	67.9	1.43	2.52	10.9	0.1	9.5
Homogenized									
1	n/a	0.245	25.7	152.8	0.64	4.69	31.4	0.1	8.4
2	n/a	0.114	25.9	131.9	2.86	4.48	19.2	0.6	9.0
3	n/a	0.068	24.2	93.7	2.64	4.27	19.2	0.1	8.3

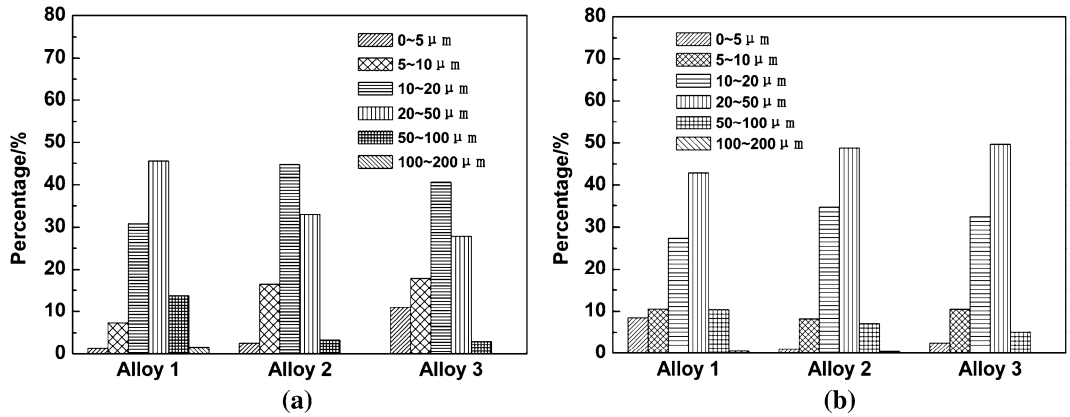

Fig. 6—Length distribution of Fe-rich phases in three 7055 alloys (*a*) as-cast alloys and (*b*) homogenized alloys.

parameters of Fe-rich phases, particularly the increase of W, imply the coarsening of the insoluble phases during homogenized at 753 K (480 °C).

Figure 6 shows the length distribution of Fe-rich phases in as-cast and homogenized 7055 alloys. In as-cast microstructures (Figure 6(a)), most of Fe-rich phases are distributed in the length range of 10 to 50 μm, with a number percentage of 70 to 75 pct for the three alloys. In addition, the proportion of coarse Fe-rich phases larger than 20 μm decreases significantly with decreasing Fe and Si contents, which results in the reduction of average length for alloy 2 and alloy 3 (Table IV). After homogenization (Figure 6(b)), the proportion of Fe-rich phases smaller than 20 μm is increased for alloy 1 but decreased for alloy 2 and alloy 3 as compared with as-cast microstructures, resulting in the reduction of average length for alloy 1, increase of average length for alloys 2 and 3, and hence very close values of L for the three alloys given in Table IV.

IV. SUMMARY AND CONCLUSIONS

Three 7055 aluminum alloys prepared by commercial-purity aluminum and high-purity aluminum of 4N and 5N as raw materials, respectively, were designed to study the influence of the variations of impurity contents on microstructural factors of second phases in as-cast and homogenized microstructure. The following conclusions can be drawn from this work:

1. In 7055 alloy cast by commercial-purity aluminum, the impurities from pure aluminum are dominant, while the impurities from master alloys of Al-50 wt pct Cu and Al-5 wt pct Zr and contamination from crucibles and tools should be controlled to ensure the high purity of 7055 alloy when cast by high-purity aluminum of 4N and 5N.
2. In as-cast microstructures of 7055 alloys with different impurity contents, the dominant second phases are coarse η phase with extended solubility of Cu and Al and dispersed η precipitates. A small

amount of impurity phases of Al_7Cu_2Fe, Al_3Fe with a little solubility of Cu, and Si and Mg_2Si are also identified, while Mg_2Si is only found in 7055 alloy with the highest contents of Fe and Si, and Fe-rich phases are usually present as the heterogeneous cores of coarse η phases. After being homogenized at 753 K (480 °C) for 24 hours, dispersed η phases are completely dissolved into the matrix and coarse η phases are largely dissolved, whereas coarse Fe-rich and Si-rich phases are insoluble and remain in the homogenized microstructures.

3. In as-cast alloys, the variations of Fe and Si contents have no significant influence on the area fraction of η phases, but the area fraction of Fe-rich phases decreases from 0.231 pct to 0.102 pct with Fe content decreasing from 0.080 wt pct to 0.038 wt pct. A further decrease of Fe content does not reduce the area fraction of Fe-rich phases any more. The size parameters of Fe-rich phases all decrease with decreasing Fe contents, and their morphology can be modified correspondingly.
4. After homogenizing, the area fractions and compositions of Fe-rich phases change a little but the morphology of Fe-rich phases are slightly coarsened.

ACKNOWLEDGMENTS

The authors would like to thank the financial support from the National Basic Research Program of China (No. 2012CB619505) and the National Natural Science Foundation of China (No. 51174135).

REFERENCES

1. A. Heinz, A. Haszler, C. Keidel, S. Moldenhauer, R. Benedictus, and W.S. Miller: *Mater. Sci. Eng. A*, 2000, vol. 280, pp. 102–07.
2. R. Ayer, J.Y. Koo, J.W. Steeds, and B.K. Park: *Metall. Trans. A*, 1985, vol. 16A, pp. 1925–36.
3. A.R. Eivani, H. Ahmed, J. Zhou, and J. Duszczyk: *Metall. Mater. Trans. A*, 2009, vol. 40A, pp. 717–28.
4. J.D. Robson: *Mater. Sci. Eng. A*, 2004, vol. 382, pp. 112–21.
5. G. Sha, Y.B. Wang, X.Z. Liao, Z.C. Duan, S.P. Ringer, and T.G. Langdon: *Mater. Sci. Eng. A*, 2010, vol. 527, pp. 4742–49.
6. Z. Cvijović, M. Rakin, M. Vratnica, and I. Cvijović: *Eng. Fract. Mech.*, 2008, vol. 75, pp. 2115–29.
7. T.F. Morgeneyer, M.J. Starink, and I. Sinclair: *Acta Mater.*, 2008, vol. 56, pp. 1671–79.
8. D. Najjar, T. Magnin, and T.J. Warner: *Mater. Sci. Eng. A*, 1997, vol. 238, pp. 293–302.
9. J. Wloka, G. Burklin, and S. Virtanen: *Electrochim. Acta*, 2007, vol. 53, pp. 2055–59.
10. F. Andreatta, H. Terryn, and J.H.W. de Wit: *Corros. Sci.,* 2003, vol. 45, pp. 1733–46.
11. N. Birbili, M.K. Cavanaugh, and R.G. Buchheit: *Corros. Sci.*, 2006, vol. 48, pp. 4202–15.
12. S.P. Knight, N. Birbilis, B.C. Muddle, A.R. Trueman, and S.P. Lynch: *Corros. Sci.*, 2010, vol. 52, pp. 4073–80.
13. G.T. Hahn and R. Rosenfield: *Metall. Trans. A*, 1975, vol. 6A, pp. 653–68.
14. D.S. Thompson: *Metall. Trans. A*, 1975, vol. 6A, pp. 671–83.
15. M. Vratnica, G. Pluvinage, P. Jodin, Z. Cvijović, M. Rakin, and Z. Burzić: *Mater. Design*, 2010, vol. 31, pp. 1790–98.
16. T. Ohira and T. Kishi: *Mater. Sci. Eng.*, 1986, vol. 78 pp. 9–19.
17. Y.B. Zuo, J.Z. Cui, J. Dong, and F.X. Yu: *J. Alloys Compd.*, 2005, vol. 402, pp. 149–55.
18. C. Mondal and A.K. Mukhopadhyay: *Mater. Sci. Eng. A*, 2005, vol. 391, pp. 367–76.
19. L.L. Rokhlin, T.V. Dobatkina, N.R. Bochvar, and E.V. Lysova: *J. Alloys Compd.*, 2004, vol. 367, pp. 10–16.
20. X.G. Fan, D.M. Jiang, Q.C. Meng, and L. Zhong: *Mater. Lett.*, 2006, vol. 60, pp. 1475–79.
21. F.Y. Xie, X.Y. Yan, L. Ding, F. Zhang, S.L. Chen, M.G. Chu, and Y.A. Chang: *Mater. Sci. Eng. A*, 2003, vol. 355, pp. 144–53.
22. Y.X. Ii, P. Li, G. Zhao, X.T. Liu, and J.Z. Cui: *Mater. Sci. Eng. A*, 2005, vol. 397, pp. 204–18.
23. N. Pourkia, M. Emamy, H. Farhangi, and S.H. Seyed Ebrahimi: *Mater. Sci. Eng. A,* 2010, vol. 527, pp. 5318–25.
24. X.M. Li and M.J. Starink: *J. Alloys Compd.*, 2011, vol. 509, pp. 471–76.
25. Y.L. Deng, L. Wan, L.H. Wu, Y.Y. Zhang, and X.M. Zhang: *J. Mater. Sci.*, 2011, vol. 46, pp. 875–81.
26. C.M. Allena, K.A.Q. O'Reilly, B. Cantor, and P.V. Evans: *Prog. Mater Sci.*, 1998, vol. 43, pp. 89–170.
27. K. Kaekwan, T. Pramote, S. Mawin, H. Nagaumi, and T. Umeda: *Int. J. Cast Metal. Res.*, 2008, vol. 21, pp. 119–24.
28. X.Y. Lv, E.J. Guo, Z.H. Li, and G.J. Wang: *Rare Met.*, 2011, vol. 30, pp. 664–68.
29. C. Freiburg and B. Grushko: *J. Alloys Compd.*, 1994, vol. 210, pp. 149–52.
30. L.F. Mondolfo: in *Aluminium Alloys: Structure and Properties.* Butterworths, London, U.K., 1976.
31. M. Asta, C. Beckermann, A. Karma, W. Kurz, R. Napolitano, M. Plapp, G. Purdy, M. Rappaz, and R. Trivedi: *Acta Mater.*, 2009, vol. 57, pp. 941–71.
32. Y. Du, Y.A. Chang, B.Y. Huang, W.P. Gong, Z.P. Jin, H.H. Xu, Z.H. Yuan, Y. Liu, Y.H. He, and F.-Y. Xie: *Mater. Sci. Eng. A*, 2003, vol. 363, pp. 140–51.